PAPER

Check for updates

A bifunctional two dimensional TM₃(HHTP)₂ monolayer and its variations for oxygen electrode reactions†

B. B. Xiao, [ID] *[a] H. Y. Liu,[a] X. B. Jiang,[b] Z. D. Yu[a] and Q. Jiang [ID] *[c]

To achieve renewable energy technologies, low-cost electrocatalysts for the oxygen reduction reaction (ORR) and the oxygen evolution reaction (OER) are required to replace Pt and IrO₂/RuO₂ catalysts. Based on density functional theory, the catalytic activity of TM₃(HHTP)₂ (2,3,6,7,10,11-hexahydroxytriphenylene) monolayer and its variations (TMX₄, where TM = Fe, Co, Ni, X = O, S, Se) for bifunctional ORR/OER have been investigated. The adsorption ability is dominated by the metal center, in the order of Fe > Co > Ni while the ligand shows the minor contribution. Due to the presence of linear relations between the intermediates, the activity of TMX₄ for the ORR/OER follows a dual volcano curve as a function of the OH adsorption strength. Considering the overpotential, CoO₄ and CoS₄ possess superior bifunctional activity, implying their promise as candidates for the oxygen electrode reaction. This systematical work may open new avenues for the development of high-performance non-PGM catalysts for practical applications of ORR and OER.

1. Introduction

There is growing interest in oxygen electrochemistry as conversions between O₂ and H₂O play important roles in renewable energy technologies, such as the rechargeable air based battery and devices that require two key electrochemical reactions, oxygen reduction (ORR) and oxygen evolution (OER).[1,2] The electrocatalytic oxygen reduction reaction (ORR) and oxygen evolution reaction (OER) play key roles in such renewable energy devices.[3] The current spectrum of catalysts utilized for these fundamental electrochemical reactions are Pt for the ORR and IrO₂ for applications in the OER.[4–6] Their "rare earth" status and associated high cost renders them less than ideal materials for incorporation into commercialization. In addition, the use of two different single function catalysts for the ORR and OER, respectively, makes the air cell significantly more complex as it requires the combination of three electrodes. In this regard, the development of active and affordable bifunctional electrocatalysts remains a challenging task.[1]

As alternatives, great efforts have been devoted to the development of the functional carbon based materials with specific atomic configuration where the heteroatom-doped, such as the nonmetallic as well as the nonprecious transition metal elements, would activate the inert C material and further boost the ORR/OER activity.[7–9] Typical example is shown by J. D. Baran *et al.* that phthalocyanines, porphyrins and their variations with the active sites composed of TMN₄ motif could be acted as the bifunctional catalysts.[10] Furthermore, S. Z. Qiao *et al.* demonstrate that the TMN₂ embedded in g-C₃N₄ promotes the oxygen electrode reactions.[2] Based on the mentioned results, the performance is obviously tuned by the selection of TM atom. However, limited investigations have been focused on the influence of the different TM/ligand combination on the activity.

The metal–organic framework (MOF) provide the abundant active sites due to the structural flexibility where the high level of individually coordinated metal and the wide selection of building block.[11,12] Besides the TM coordinated with N ligand, other combinations within MOF have been experimentally synthesized,[13–16] such as the uniform distribution of TMS₄ and TMO₄ motifs,[14,16] which could offer the prototype for the investigation of the TM/ligand effect. On the other hand, inspired by the attractive bifunctional electrocatalysis exhibited by the TM dichalcogenides,[17–20] the active centers consisted by the TM coordinated to the O/S/Se atoms have raised our attention as the ORR/OER electrode.

To classify the effect of the mentioned combinations, the primary consideration is the theoretical model where the TM₃(HHTP)₂ monolayer is selected as the prototype in our investigation.[16] In the regard, DFT calculations are used within the electrochemical framework to analyze the ORR/OER

[a]School of Energy and Power Engineering, Jiangsu University of Science and Technology, 212003, Zhenjiang, Jiangsu, China. E-mail: xiaobb11@mails.jlu.edu.cn

[b]School of Materials Science and Engineering, Jiangsu University of Science and Technology, 212003, Zhenjiang, Jiangsu, China

[c]Key Laboratory of Automobile Materials (Jilin University), Ministry of Education, School of Materials Science and Engineering, Jilin University, Changchun 130022, China. E-mail: jiangq@jlu.edu.cn

† Electronic supplementary information (ESI) available. See DOI: 10.1039/c7ra09974f

reaction. The $TM_3(HHTP)_2$ prototype and its variations have been systemically studied to illustrate the critical role of the metal/ligand combination, where the schematic monolayer structures are shown in Fig. 1(a). The corresponding stability of the reaction intermediates is considered, which allows for the evaluation of the free energy and overpotentials. Based on the information, the bifunctional candidates are screened out by a thorough comparison.

2.   Computational method

All calculations are performed within the DFT framework as implemented in $DMol^3$ code.[21,22] The generalized gradient approximation with the Perdew–Burke–Ernzerhof (PBE) functional is employed to describe exchange and correlation effects.[23] The DFT semi-core pseudopots (DSPP) core treat method is implemented for relativistic effects, which replace core electrons by a single effective potential and introduce some degree of relativistic correction into the core.[24] The double numerical atomic orbital augmented by a polarization function (DNP) is chosen as the basis set.[21] A smearing of 0.005 Ha (1 Ha = 27.21 eV) to the orbital occupation is applied to achieve accurate electronic convergence. In order to ensure high-quality results, the real-space global orbital cutoff radius is set as high as 5.2 Å. In the geometry structural optimization, the convergence tolerances of energy, maximum force and displacement are 1.0×10^{-5} Ha, 0.002 Ha Å^{-1} and 0.005 Å, respectively. The spin-unrestricted method is used for all calculations. A conductor-like screening model (COSMO) was used to simulate a H_2O solvent environment for all calculations,[25] which is a continuum model where the solute molecule forms a cavity within the dielectric continuum. The $DMol^3$/COSMO method has been generalized to periodic boundary cases. The dielectric constant is set as 78.54 for H_2O. Some previous results have shown that this implicit solvation model is an effective method to describe solvation.[15,26] The 15 Å-thick vacuum is added to avoid the artificial interactions between the nanosheet and its images.

In the reaction energy landscape, all ORR/OER intermediates are described as proton/electron ($H^+ + e^-$) transfers.[4,5] The adsorption energy of the corresponding intermediates are calculated by the following,[10]

$$E_{ORR}(OOH) = E_{OOH} - E_{substrate} - E_{O_2} - (H^+ + e^-) \quad (1)$$

$$E_{ORR}(O) = E_O - E_{substrate} - 1/2E_{O_2} + H_f(H_2O) \quad (2)$$

$$E_{ORR}(OH) = E_{OH} - E_{substrate} - 1/2E_{O_2} - (H^+ + e^-) + H_f(H_2O) \quad (3)$$

where E_{sys}, $E_{substrate}$, E_{H_2O}, E_{O_2} and E_{H_2} are the total energy of the adsorption systems, the $TM_3(HITP)_2$ monolayer, H_2O molecule, O_2 molecule and H_2 molecule, respectively. $E_{ORR} < 0$ corresponds to an exothermic adsorption process.

To study the ORR/OER activity, the Gibbs free energy changes (ΔG) of the ORR elemental steps have been calculated according to the computational hydrogen electrode (CHE) model developed by Nørskov et al. where the chemical potential of proton/electron ($H^+ + e^-$) in solution is equal to the half of the chemical potential of a gas-phase H_2.[4] The ΔG for every elemental step can be determined as following:

$$\Delta G = \Delta E + \Delta ZPE - T\Delta S + \Delta G_{pH} + \Delta G_U \quad (4)$$

where ΔE is the electronic energy difference based on DFT calculations, ΔZPE is the change in zero point energy, T is the temperature (equal to 298.15 K here), ΔS is the change in the entropy, and ΔG_{pH} and ΔG_U are the free energy contributions due to variation in pH value (pH is set as 0 in acid medium) and electrode potential U, respectively. In order to decrease the calculation consumption, the approximate correction $\Delta ZPE - T\Delta S$ to ΔE (0.05/0.30/0.35 eV of O*/OH*/OOH*) are used for constructed the ΔG. As OER are reverse process of the ORR, the corresponding ΔG of OER intermediates are calculated in the following equation:

$$\Delta G_{OER}(M) = \Delta G_{ORR}(M) + 4.92 \quad (5)$$

The thermodynamic CHE model has been applied to interpret the experimental data and design the novel electrocatalysts for metal, oxides as well as carbon-based materials.[10,15,27–32] Besides, the present computational method has been applied to illustrate the ORR mechanism of the $TM_3(HITP)_2$ (HITP = hexaiminotriphenylene) monolayer. Therein, the $2e^-$ mechanism is predicted to be prevalent for $Ni_3(HITP)_2$ system owing to the insufficient O_2 activation, which is in accordance with the experimental data established by E. M. Miner.[33] Therefore, considered the structural similarity of the $TM_3(HITP)_2$ and $TM_3(HHTP)_2$ systems, the reliability of our calculation could be confirmed. However, it should be realized that the material stability under the harsh electrochemical environment has been neglected herein. Despite the bifunctional ORR/OER electrocatalytic candidates have been screened out based on our theoretical trend, further performance needs the experimental confirmation.

3.   Results and discussion

The favorable adsorption properties of the ORR/OER intermediates are the prerequisite for the reaction proceeding. The corresponding adsorption energies are tabulated in Table 1. It
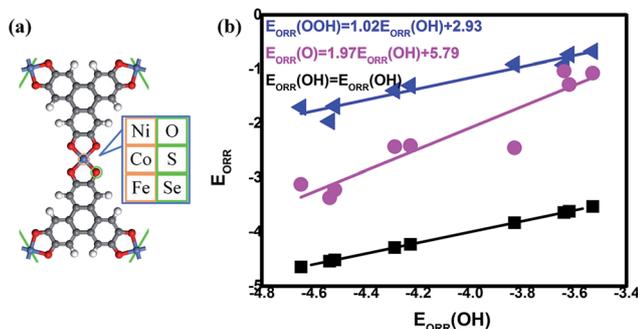

Fig. 1   The schematic structure (a) and the corresponding adsorption energy of ORR/OER intermediates (b).

should be point out that the values do not signify the absolute strength of the intermediates adsorption. As shown, the adsorption energy decreases monotonically with increasing the d-electron in the valence shell of the metal center, which could be accounted by the d-band model.[34] That is, the adsorption ability is tuned by the variation of the metal center, following the order of Fe > Co > Ni.[2,15,35] In order to reveal the ligand effect, the corresponding Mulliken charges of the TM active center as well as the ORR intermediates are plotted in Fig. 2 where positive and negative represent charge depletion and accumulation, respectively. As shown in Fig. 2(a), the charge is transferred from the TM atom to the C-based skeleton for the TMO_4 systems without adsorption, indicating the charge depletion of the TM active center for NiO_4, CoO_4 and FeO_4, respectively meanwhile the charge accumulation is found for the other two systems, especially for CoS_4 and $CoSe_4$. On the other hand, interacted with the ORR intermediates, the phenomenon of the charge depletion for NiO_4, CoO_4 and FeO_4 in combination with the charge accumulation of CoS_4 and $CoSe_4$ are remained, being similar compared with the un-adsorbed systems. However, for NiS_4, $NiSe_4$, FeS_4 and $FeSe_4$, the generally tendency of the charge accumulation before adsorption changed toward to the charge depletion with ORR intermediates adsorption is observed. Herein, the ligand effect of the charge distribution possesses the similar behavior on the certain degrees for the TMS_4 and $TMSe_4$, as implied by Fig. 2(a). The point is further supported by the partially density of states (PDOS). For CoX_4 as shown in Fig. 3, the appearance of the p-orbital ranged from -3 eV to the Fermi energy is observed for CoS_4 and $CoSe_4$, which is missed for the CoO_4. Besides, the sharp double d-peaks are located at ~ -1.6 eV and -1.0 eV for the former systems, being different from the d-peaks of the CoO_4, which confirms the variation of the d-orbital as the ligand charged. The similarity is found for NiX_4 and FeX_4, where the detail PDOS plots are shown in Fig. S1 and S2 of the ESI.† As discussed, the charge analysis as well as PDOS morphology demonstrates the complex ligand effect on the subtle electronic structure of the TM active center, being dependent on the TM element selection, which would lead to the variation of the adsorption energy. Taken Co combination as an example, the neglect variation is found for $E_{ORR}(O)$ as the ligand changes.

However, the $E_{ORR}(OOH)$ and $E_{ORR}(OH)$ are significantly weakened as the ligand varied from O/S to Se. The situation is completely different for the Ni/Fe combination. As shown in Fig. 2, due to the charge transfer, the ionic bonding between the O-containing species is formed.[36] The charge accumulations of the Co active center and the O-containing species are observed, implying the presence of electrostatic repulsion, which is different from the situations between Ni/Fe and the ORR intermediates with the electrostatic attraction.[37,38] It is plausibly accounted for the mentioned weakening phenomenon for CoX_4. On the other hand, it should been noted that the covalent bonds are dominated by the interaction of the O-p orbital and the TM-d orbital, in combination with the minor contribution of the p–p orbital overlap demonstrated in Fig. 3 as well as Fig. S1 and S2.† Herein, both covalent bonds due to the overlap of orbitals and ionic bonds induced by the charge transfer influence the adsorption.[36] Due to the difference of the electronic structures, the general trend of the ligand effect is difficultly summarized.

The data could be plotted as a function of OH adsorption, as shown in Fig. 1(b). From our results, the universal linear relationships between the ORR intermediates are clearly observed, which is in agreement with the previous studies.[10,15,35,39] That is,

$$E_{ORR}(OOH) = 1.02 E_{ORR}(OH) + 2.93 \qquad (6)$$

$$E_{ORR}(O) = 1.97 E_{ORR}(OH) + 5.79 \qquad (7)$$

Compared with the previous data of the porphyrins analogues,[10] it is found that the slopes of the fitting lines are comparable. It should be noted that the data deviation of $CoSe_4$ [$E_{ORR}(O) = -2.45$ eV, $E_{ORR}(OH) = -3.83$ eV] from the scaling relation between $E_{ORR}(O)$ and $E_{ORR}(OH)$ is obvious. Such deviation could be observed in the C-based electrocatalysts,[10,15,35] which is caused by the different electron transfer required for ORR intermediates adsorption (formally 2e/1e for O/OH, respectively).[10] Herein, our Mulliken charge analysis shows the consistence with the statement where the adsorbed O possesses the more electrons compared with the adsorbed OH, indicated by the values shown in Fig. 2(b). Furthermore, the intercept of $E_{ORR}(OOH)$ *vs.* $E_{ORR}(OH)$ generally approaches 3.2 eV, regardless the catalytic materials.[10,31,35,39] Herein, it is well-known that the mentioned scaling relations allow the dependence of the ORR activity on the adsorption strength that too strong means the poisoning of the O-containing species whereas too weak implies the insufficient activation ability, both of which is considered as the origin the ORR overpotential.[4,40]

To evaluate the activity of the mentioned systems, the OOH associative mechanisms are taken into consideration with the elemental steps R_i listing in the following,[10,35] where asterisks denote active TM sites. Due to the small barrier of proton transfer, which could be ignored at high applied voltages, our attentions are only are focused on the reaction energies.[4,15,35,41] The corresponding free energy value G is analyzed and depicted in Fig. 4. As shown by the following equations, the four-electron ORR pathways in OOH association mechanism can proceed through OOH formation (R_1), O formation (R_2), OH formation (R_3) and H_2O formation (R_4).

Table 1 The adsorption energy of ORR intermediates (E_{ORR}) and Gibbs free energies of the ORR/OER intermediates. All results are in units of eV

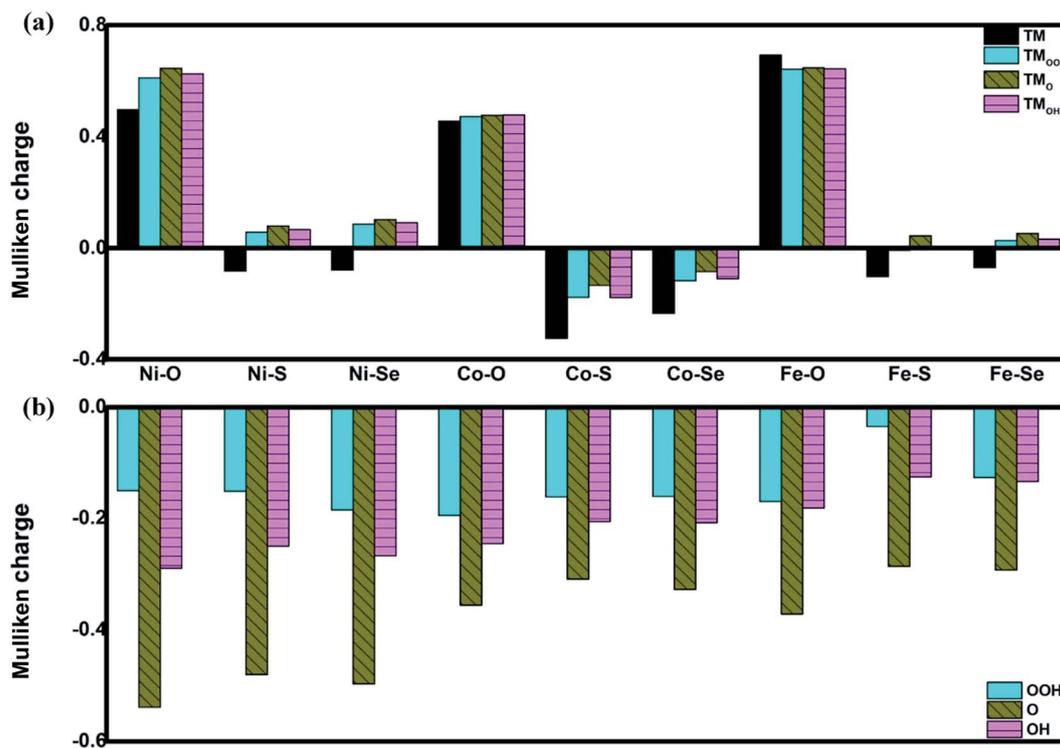|	EORR			GOER			GORR		
	OOH	O	OH	OOH	O	OH	OOH	O	OH
Ni–O	−0.92	−1.03	−3.64	−0.57	−0.98	−3.34	4.35	3.94	1.58
Co–O	−1.39	−2.43	−4.29	−1.04	−2.38	−3.99	3.88	2.54	0.93
Fe–O	−1.70	−3.12	−4.65	−1.35	−3.07	−4.35	3.57	1.85	0.57
Ni–S	−0.67	−1.07	−3.53	−0.32	−1.02	−3.23	4.60	3.90	1.69
Co–S	−1.30	−2.41	−4.23	−0.95	−2.36	−3.93	3.97	2.56	0.99
Fe–S	−1.68	−3.22	−4.52	−1.33	−3.17	−4.22	3.59	1.75	0.70
Ni–Se	−0.73	−1.28	−3.62	−0.38	−1.23	−3.32	4.54	3.69	1.60
Co–Se	−0.91	−2.45	−3.83	−0.56	−2.40	−3.53	4.36	2.52	1.39
Fe–Se	−1.96	−3.37	−4.54	−1.26	−3.32	−4.24	3.66	1.60	0.68

Fig. 2 The Mulliken charge of the TM active center (a) and the ORR intermediates (b). TM denotes the un-adsorbed TM atom while TM_{OOH}, TM_O and TM_{OH} are the OOH, O and OH adsorbed TM atom, respectively.
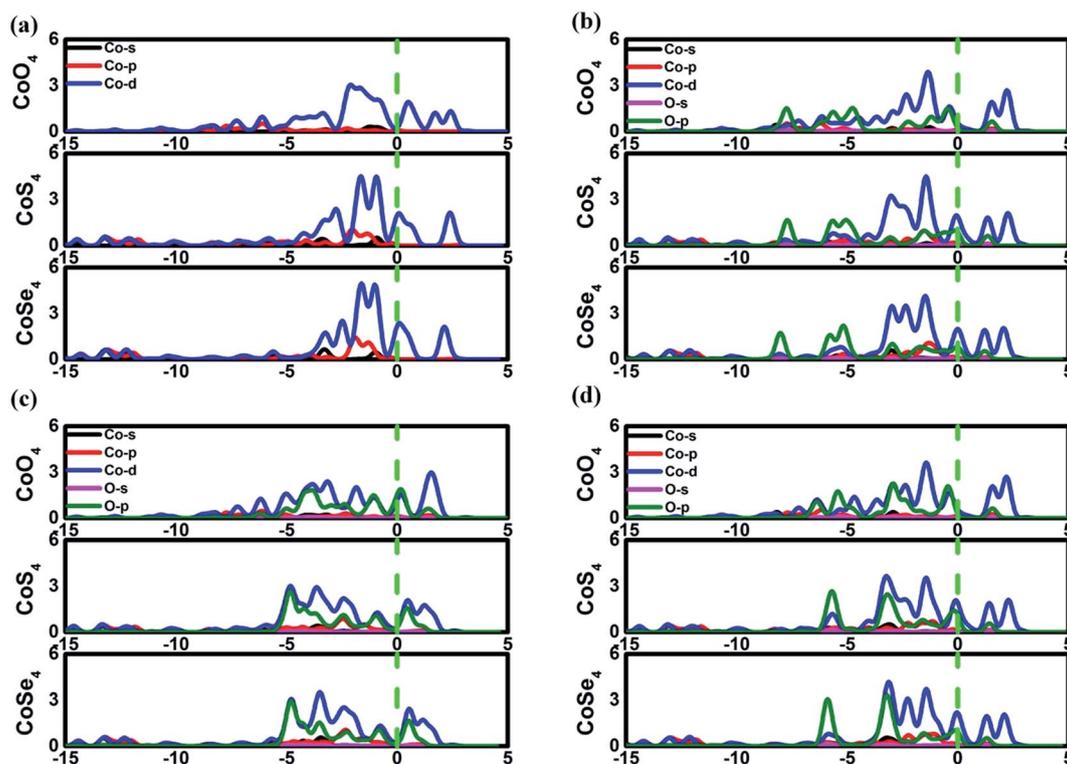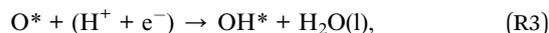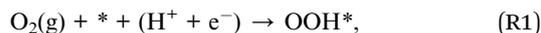

Fig. 3 The partially density of states of $Co_3(HHTP)_2$ and its variations. (a) is the un-adsorbed CoX_4. (b), (c) and (d) are OOH, O and OH adsorption systems, respectively.

$$O_2(g) + * + (H^+ + e^-) \rightarrow OOH^*, \qquad (R1)$$

$$OOH^* + (H^+ + e^-) \rightarrow O^* + H_2O(l), \qquad (R2)$$

$$O^* + (H^+ + e^-) \rightarrow OH^* + H_2O(l), \qquad (R3)$$

$$OH^* + (H^+ + e^-) \rightarrow 2H_2O(l). \qquad (R4)$$

From the figures, for NiO_4 monolayer, the whole elemental steps are exothermic at the potential U of 0 V, indicating the thermodynamic favor. However, as the U is raised to 1.23 V, the situation is changed that (R_1) and (R_2) become endothermic, respectively, implying the ORR reaction would be not proceeded spontaneously. For clearly observation, the ΔG values are gathered in Table 2. Herein, the rate-determining step (RDS) with the largest ΔG_{max} value could be acted as a measure of the catalyst activity.[4] The RDS is located at (R_2) with ΔG_{max} of 0.82 eV for NiO_4 monolayer at 1.23 V. Furthermore, other catalytic materials possess good activity at 0 V without the endothermic reaction steps while the unfavorable thermodynamics are observed at 1.23 V, being similar with NiO_4 monolayer. However, it should be

Table 2   Gibbs free energies changes of the elemental steps for ORR at the potential U of 0 and 1.23 V

	$U = 0$ V				$U = 1.23$ V			
	R_1	R_2	R_3	R_4	R_1	R_2	R_3	R_4
Ni–O	−0.57	−0.41	−2.36	−1.58	0.66	0.82	−1.13	−0.35
Co–O	−1.04	−1.34	−1.61	−0.93	0.19	−0.11	−0.38	0.30
Fe–O	−1.35	−1.72	−1.28	−0.57	−0.12	−0.49	−0.05	0.66
Ni–S	−0.32	−0.71	−2.21	−1.69	0.91	0.52	−0.98	−0.46
Co–S	−0.95	−1.40	−1.57	−0.99	0.28	−0.17	−0.34	0.24
Fe–S	−1.33	−1.84	−1.05	−0.70	−0.10	−0.61	0.18	0.53
Ni–Se	−0.38	−0.85	−2.09	−1.60	0.85	0.38	−0.86	−0.37
Co–Se	−0.56	−1.84	−1.13	−1.39	0.67	−0.61	0.10	−0.16
Fe–Se	−1.26	−2.06	−0.92	−0.68	−0.03	−0.83	0.31	0.55

noted that two different RDS could be identified. That is, (R_1) is for NiS_4, $NiSe_4$, CoS_4, $CoSe_4$ with the ΔG_{max} of 0.91, 0.28, 0.85 and 0.67 eV while (R_4) is for CoO_4, FeO_4, FeS_4, $FeSe_4$ with the ΔG_{max} of 0.30, 0.66, 0.53 and 0.55 eV, respectively.

Based on the free energy profiles, the highest potential for the feasible thermodynamic ORR steps are obtained and its
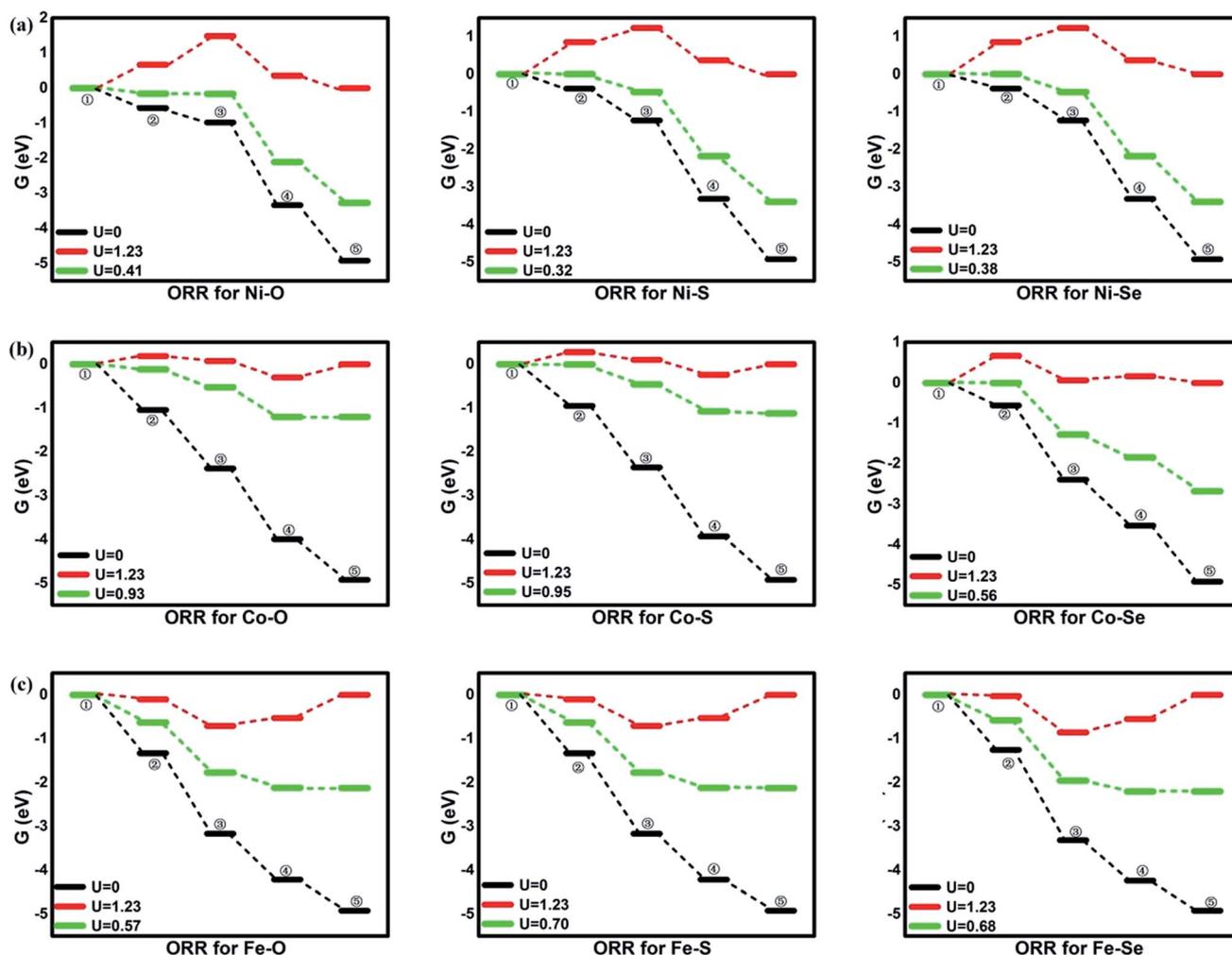

Fig. 4   The free energy of ORR. ①: $O_2 + 4(H^+ + e^-)$; ②: $*OOH + 3(H^+ + e^-)$; ③: $*O + H_2O + 2(H^+ + e^-)$; ④: $*OH + H_2O + (H^+ + e^-)$; ⑤: $2H_2O$.

Table 3 The overpotential of the intermediates for ORR and OER

	μ_{ORR}	μ_{OER}
Ni–O	0.82	−1.13
Co–O	0.30	−0.38
Fe–O	0.66	−0.49
Ni–S	0.91	−0.98
Co–S	0.28	−0.34
Fe–S	0.53	−0.61
Ni–Se	0.85	−0.86
Co–Se	0.67	−0.61
Fe–Se	0.55	−0.83

corresponding overpotential μ_{ORR} are summarized in Table 3. The ORR activity follows the order of $CoS_4(0.28) \approx CoO_4(0.30) > FeS_4(0.53) \approx FeSe_4(0.55) > FeO_4(0.66) \approx CoSe_4(0.67) > NiO_4(0.82) \approx NiSe_4(0.85) \approx NiS_4(0.91)$. From the data, the relative minor dependence of the activity on the coordinated ligand of the Ni and Fe active sites is observed. The corresponding μ_{ORR} changes are less than 0.10 V and 0.15 V, respectively. However, for Co metal center, the μ_{ORR} of the $CoSe_4$ are much higher than those of CoS_4 and CoO_4, indicating the importance of the ligand selection. On the other hand, the effect of the metal center on the

ORR activity is obvious. Generally, the inferior/moderate activities are found for the Ni/Fe combination. For the Co active centers, the superior performances of the CoO_4 and CoS_4 are found referred to the current Pt with the μ_{ORR} of 0.45 V.[4]

As discussed by the previous reports,[10,15,35,39] the ORR activity depends on the adsorption of the intermediates. Due to the linear relationship between the adsorption of ORR intermediates and the OH, the overpotential μ_{ORR} as a function of the $E_{ORR}(OH)$ is described in Fig. 6. As the enhancement of the adsorption ability, the μ_{ORR} reduces and then increase, demonstrating the classical volcano-shaped activity is found.[2,4,10,35] For NiO_4, NiS_4, $NiSe_4$ and $CoSe_4$ with weak adsorption strength, the high μ_{ORR} originates from the ineffective weakening the O–O coupling. For Fe combination located at the branch of the strong adsorption, the OH poisoning accounts for the increased μ_{ORR}. Due to the suitable adsorption ability, the CoO_4 and CoS_4 are situated at the apex of the volcano curve. Our results are in accordance with the previous reports that the bond strength should be compromised for the effective ORR catalysts on the basis of Sabatier principle.[40]

Besides the ORR activity, the OER activity is characterized in Fig. 5 where the reversed process of the OOH associative mechanisms is considered. The free energy of OER intermediates are obtained by the eqn (5) and the corresponding data are
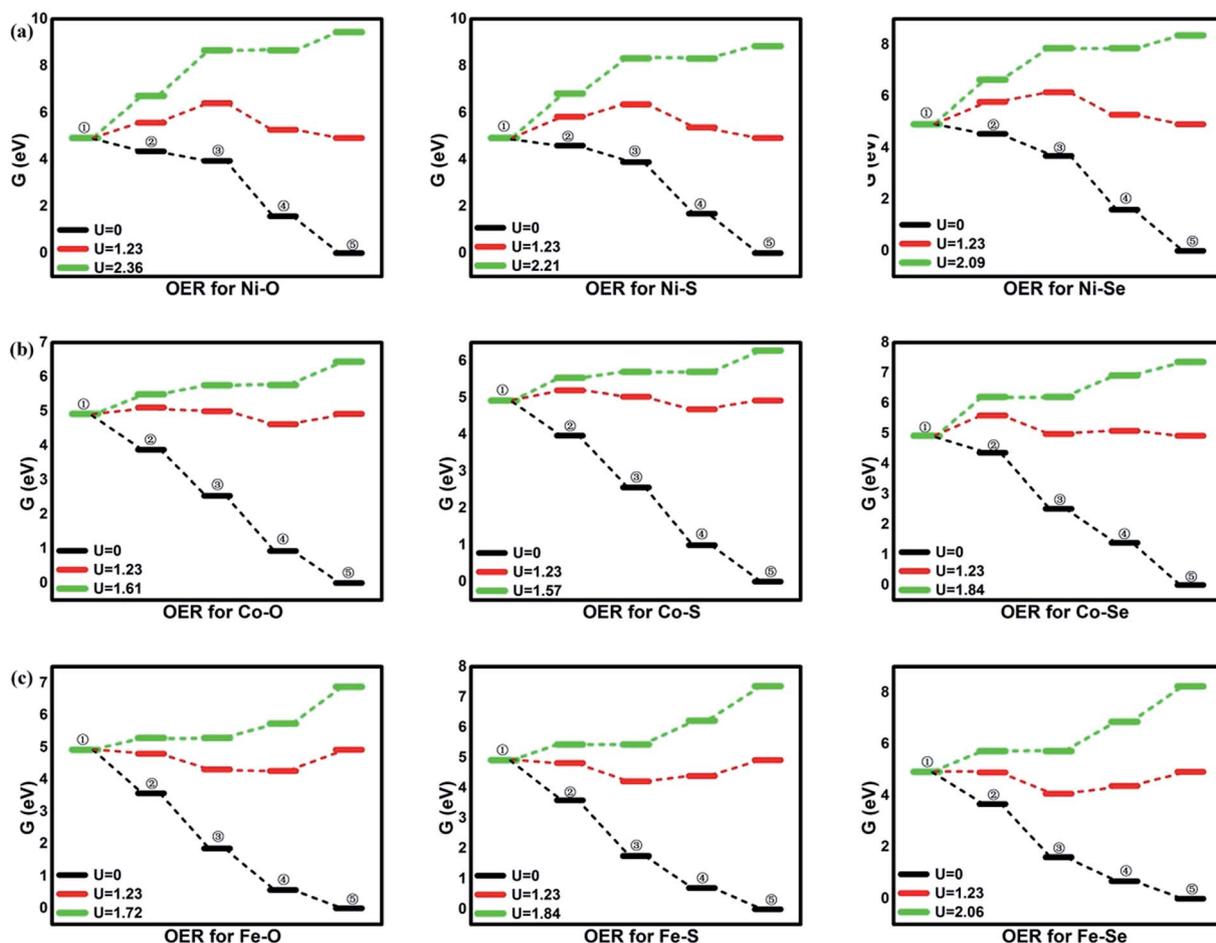

Fig. 5 The free energy of OER. ①: $O_2 + 4(H^+ + e^-)$; ②: $*OOH + 3(H^+ + e^-)$; ③: $*O + H_2O + 2(H^+ + e^-)$; ④: $*OH + H_2O + (H^+ + e^-)$; ⑤: $2H_2O$.
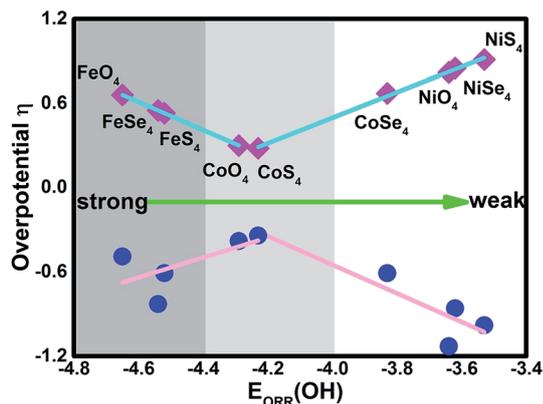
Fig. 6 The dual volcano plot of the overpotential as a function of the OH adsorption energy for ORR and OER.

shown in Table 2. From our results, no OER activity could be found at 1.23 V where the reaction steps are thermodynamically hindered due to the endothermic characterization. The RDS are located at the OH* oxidation (the reserve (R_3)) for NiO_4, NiS_4, $NiSe_4$, CoO_4, CoS_4 and the OOH* formation from the adsorbed O* (the reserve (R_2)) for $CoSe_4$, FeO_4, FeS_4, $FeSe_4$, respectively. As shown, the unfavorable endothermic steps are changed to be exothermic as the potential U increases. The corresponding equilibrium potentials are in the order of $NiO_4(2.36) > NiS_4(2.21) > NiSe_4(2.09) \approx FeSe_4(2.06) > FeS_4(1.84) = CoSe_4(1.84) > FeO_4(1.72) > CoO_4(1.61) \approx CoS_4(1.57)$. Herein, for clear observation, the overpotential μ_{OER} are collected in Table 3 and its $E_{ORR}(OH)$-dependence is shown in Fig. 6 where the volcano-curve is roughly observed.[2,10] Too weak or too strong $E_{ORR}(OH)$ leads to the high μ_{OER} and then the inferior activity. The CoO_4 and CoS_4 possess the superior activity the minimum μ_{OER} with the values of 0.38 and 0.34 V, in comparison with the IrO_2 of 0.56 V, respectively.[5]

Based on the mentioned results, CoX_4 show the bests activity with the exception of $CoSe_4$ due to the too weak capture ability of the reaction intermediates. Herein, the CoO_4 and CoS_4 are identified as the high efficient electrocatalysts to replace Pt for ORR and IrO_2/RuO_2 for OER. Besides, FeX_4 provides better activity in comparison with NiX_4. Generally, the reversible ORR/OER activity is mainly relied on the selection of the metal center. The different ligand gives slightly tuned. Herein, our stimulation provides the potential candidates for experimental synthesis. However, the structural stability as well as its conductivity are not concerned and out of our scope. Furthermore, due to the structure-dependence property, the model selection leads to distinct possibility for electrocatalysis application. Therefore, due to the limited work, extending our results to the whole MOF systems is not suitable.

4.   Conclusion

Based on density functional theory, ORR/OER activity on a TMX_4 monolayer has been systematically studied. It is found that the combination of the metal center and the ligand affects the ORR/OER bifunctional activity where the classical volcano-curve as a function of $E_{ORR}(OH)$ is roughly observed. Furthermore, based on the overpotential obtained from the free energy profiles, the ORR activity follows the order of $CoS_4 \approx CoO_4 > FeS_4 \approx FeSe_4 > FeO_4 \approx CoSe_4 > NiO_4 \approx NiSe_4 \approx NiS_4$ while the OER activity follows the order of $CoS_4 \approx CoO_4 > FeO_4 > CoSe_4 = FeS_4 > FeSe_4 \approx NiSe_4 > NiS_4 > NiO_4$, suggesting that CoO_4 and CoS_4 exhibit the superior catalytic activity. These results may serve as guidance for rational material design and synthesis.

Conflicts of interest

There are no conflicts to declare.

Acknowledgements

References

1 Y. Gorlin and T. F. Jaramillo, A Bifunctional Nonprecious Metal Catalyst for Oxygen Reduction and Water Oxidation, *J. Am. Chem. Soc.*, 2010, **132**, 13612–13614.

2 Y. Zheng, Y. Jiao, Y. Zhu, Q. Cai, A. Vasileff, L. H. Li, Y. Han, Y. Chen and S. Z. Qiao, Molecule-Level g-C_3N_4 Coordinated Transition Metals as a New Class of Electrocatalysts for Oxygen Electrode Reactions, *J. Am. Chem. Soc.*, 2017, **139**, 3336–3339.

3 Y. Zhao, K. Kamiya, K. Hashimoto and S. Nakanishi, Efficient Bifunctional Fe/C/N Electrocatalysts for Oxygen Reduction and Evolution Reaction, *J. Phys. Chem. C*, 2015, **119**, 2583–2588.

4 J. K. Nørskov, J. Rossmeisl, A. Logadottir, L. Lindqvist and J. R. Kitchin, Origin of the Overpotential for Oxygen Reduction at a Fuel-Cell Cathode, *J. Phys. Chem. B*, 2004, **108**, 17886–17892.

5 J. Rossmeisl, Z. W. Qu, H. Zhu, G. J. Kroes and J. K. Nørskov, Electrolysis of water on oxide surfaces, *J. Electroanal. Chem.*, 2007, **607**, 83–89.

6 F. D. Kong, S. Zhang, G. P. Yin, N. Zhang, Z. B. Wang and C. Y. Du, Pt/porous-IrO_2 nanocomposite as promising electrocatalyst for unitized regenerative fuel cell, *Electrochem. Commun.*, 2012, **14**, 63–66.

7 Y. Jiao, Y. Zheng, M. Jaroniec and S. Z. Qiao, Design of electrocatalysts for oxygen- and hydrogen-involving energy conversion reactions, *Chem. Soc. Rev.*, 2015, **44**, 2060–2086.

8 Z. Chen, D. Higgins, A. Yu, L. Zhang and J. Zhang, A review on non-precious metal electrocatalysts for PEM fuel cells, *Energy Environ. Sci.*, 2011, **4**, 3167–3192.

9 M. Tahir, L. Pan, F. Idrees, X. Zhang, L. Wang, J. J. Zou and Z. L. Wang, Electrocatalytic oxygen evolution reaction for energy conversion and storage: A comprehensive review, *Nano Energy*, 2017, **37**, 136–157.

10 J. D. Baran, H. Grönbeck and A. Hellman, Analysis of Porphyrines as Catalysts for Electrochemical Reduction of

O$_2$ and Oxidation of H$_2$O, *J. Am. Chem. Soc.*, 2014, **136**, 1320–1326.

11 A. Zarkadoulas, M. J. Field, V. Artero and C. A. Mitsopoulou, Proton-Reduction Reaction Catalyzed by Homoleptic Nickel-bis-1,2-dithiolate Complexes: Experimental and Theoretical Mechanistic Investigations, *ChemCatChem*, 2017, **9**, 2308–2317.

12 J. J. Perry IV, J. A. Perman and M. J. Zaworotko, Design and synthesis of metal–organic frameworks using metal–organic polyhedra as supermolecular building blocks, *Chem. Soc. Rev.*, 2009, **38**, 1400–1417.

13 T. Kambe, R. Sakamoto, K. Hoshiko, K. Takada, M. Miyachi, J. H. Ryu, S. Sasaki, J. Kim, K. Nakazato, M. Takata and H. Nishihara, π-Conjugated Nickel Bis(dithiolene) Complex Nanosheet, *J. Am. Chem. Soc.*, 2013, **135**, 2462–2465.

14 A. J. Clough, J. W. Yoo, M. H. Mecklenburg and S. C. Marinescu, Two-Dimensional Metal–Organic Surfaces for Efficient Hydrogen Evolution from Water, *J. Am. Chem. Soc.*, 2015, **137**, 118–121.

15 P. Zhang, X. Hou, L. Liu, J. Mi and M. Dong, Two-Dimensional π-Conjugated Metal Bis(dithiolene) Complex Nanosheets as Selective Catalysts for Oxygen Reduction Reaction, *J. Phys. Chem. C*, 2015, **119**, 28028–28037.

16 M. G. Campbell, S. F. Liu, T. M. Swager and M. Dincă, Chemiresistive sensor arrays from conductive 2D metal–organic frameworks, *J. Am. Chem. Soc.*, 2015, **137**, 13780–13783.

17 Q. Liu, J. Jin and J. Zhang, NiCo$_2$S$_4$@Graphene as a Bifunctional Electrocatalyst for Oxygen Reduction and Evolution Reactions, *ACS Appl. Mater. Interfaces*, 2013, **5**, 5002–5008.

18 P. Ganesan, M. Prabu, J. Sanetuntikul and S. Shanmugam, Cobalt Sulfide Nanoparticles Grown on Nitrogen and Sulfur Codoped Graphene Oxide: An Efficient Electrocatalyst for Oxygen Reduction and Evolution Reactions, *ACS Catal.*, 2015, **5**, 3625–3637.

19 J. A. Koza, Z. He, A. S. Miller and J. A. Switzer, Electrodeposition of Crystalline Co$_3$O$_4$—A Catalyst for the Oxygen Evolution Reaction, *Chem. Mater.*, 2012, **24**, 3567–3573.

20 Y. Liu, H. Cheng, M. Lyu, S. Fan, Q. Liu, W. Zhang, Y. Zhi, C. Wang, C. Xia, S. Wei, B. Ye and Y. Xie, Low Overpotential in Vacancy-Rich Ultrathin CoSe$_2$ Nanosheets for Water Oxidation, *J. Am. Chem. Soc.*, 2014, **136**, 15670–15675.

21 B. Delley, An all-electron numerical method for solving the local density functional for polyatomic molecules, *J. Chem. Phys.*, 1990, **92**, 508–517.

22 B. Delley, From molecules to solids with the DMol^3 approach, *J. Chem. Phys.*, 2000, **113**, 7756–7764.

23 J. P. Perdew, K. Burke and M. Ernzerhof, Generalized Gradient Approximation Made Simple, *Phys. Rev. Lett.*, 1996, **77**, 3865–3868.

24 B. Delley, Hardness conserving semilocal pseudopotentials, *Phys. Rev. B: Condens. Matter Mater. Phys.*, 2002, **66**, 155125.

25 T. Todorova and B. Delley, Wetting of paracetamol surfaces studied by DMol^3–COSMO calculations, *Mol. Simul.*, 2008, **34**, 1013–1017.

26 Y. Sha, T. H. Yu, B. V. Merinov, P. Shirvanian and W. A. Goddard, Oxygen Hydration Mechanism for the Oxygen Reduction Reaction at Pt and Pd Fuel Cell Catalysts, *J. Phys. Chem. Lett.*, 2011, **2**, 572–576.

27 I. E. L. Stephens, A. S. Bondarenko, U. Grønbjerg, J. Rossmeisl and I. Chorkendorff, Understanding the electrocatalysis of oxygen reduction on platinum and its alloys, *Energy Environ. Sci.*, 2012, **5**, 6744–6762.

28 D. H. Lee, W. J. Lee, W. J. Lee, S. O. Kim and Y. H. Kim, Theory, Synthesis, and Oxygen Reduction Catalysis of Fe-Porphyrin-Like Carbon Nanotube, *Phys. Rev. Lett.*, 2011, **106**, 175502.

29 M. Favaro, L. Ferrighi, G. Fazio, L. Colazzo, C. Di Valentin, C. Durante, F. Sedona, A. Gennaro, S. Agnoli and G. Granozzi, Single and Multiple Doping in Graphene Quantum Dots: Unraveling the Origin of Selectivity in the Oxygen Reduction Reaction, *ACS Catal.*, 2015, **5**, 129–144.

30 Y. Jia, L. Zhang, A. Du, G. Gao, J. Chen, X. Yan, C. L. Brown and X. Yao, Defect Graphene as a Trifunctional Catalyst for Electrochemical Reactions, *Adv. Mater.*, 2016, **28**, 9532–9538.

31 I. C. Man, H. Y. Su, F. Calle-Vallejo, H. A. Hansen, J. I. Martínez, N. G. Inoglu, J. Kitchin, T. F. Jaramillo, J. K. Nørskov and J. Rossmeisl, Universality in Oxygen Evolution Electrocatalysis on Oxide Surfaces, *ChemCatChem*, 2011, **3**, 1159–1165.

32 X. Y. Lang, G. F. Han, B. B. Xiao, L. Gu, Z. Z. Yang, Z. Wen, Y. F. Zhu, M. Zhao, J. C. Li and Q. Jiang, Mesostructured Intermetallic Compounds of Platinum and Non-transition Metals for Enhanced Electrocatalysis of Oxygen Reduction Reaction, *Adv. Funct. Mater.*, 2015, **25**, 230–237.

33 E. M. Miner, T. Fukushima, D. Sheberla, L. Sun, Y. Surendranath and M. Dincă, Electrochemical oxygen reduction catalysed by Ni$_3$(hexaiminotriphenylene)$_2$, *Nat. Commun.*, 2016, **7**, 10942.

34 B. Hammer and J. K. Nørskov, Theoretical surface science and catalysis—calculations and concepts, *Adv. Catal.*, 2000, **45**, 71–129.

35 F. Calle-Vallejo, J. I. Martínez and J. Rossmeisl, Density functional studies of functionalized graphitic materials with late transition metals for oxygen reduction reactions, *Phys. Chem. Chem. Phys.*, 2011, **13**, 15639–15643.

36 W. Liu, Y. F. Zhu, J. S. Lian and Q. Jiang, Adsorption of CO on Surfaces of 4d and 5d Elements in Group VIII, *J. Phys. Chem. C*, 2007, **111**, 1005–1009.

37 P. J. Feibelman, d-electron frustration and the large fcc *versus* hcp binding preference in O adsorption on Pt(111), *Phys. Rev. B: Condens. Matter Mater. Phys.*, 1997, **56**, 10532.

38 M. T. M. Koper and R. A. van Santen, Interaction of H, O and OH with metal surfaces, *J. Electroanal. Chem.*, 1999, **472**, 126–136.

39 V. Viswanathan, H. A. Hansen, J. Rossmeisl and J. K. Nørskov, Universality in Oxygen Reduction Electrocatalysis on Metal Surfaces, *ACS Catal.*, 2012, **2**, 1654–1660.

40 J. Greeley, I. E. L. Stephens, A. S. Bondarenko, T. P. Johansson, H. A. Hansen, T. F. Jaramillo, J. Rossmeisl, I. Chorkendorff and J. K. Nørskov, Alloys of platinum and early transition metals as oxygen reduction electrocatalysts, *Nat. Chem.*, 2009, **1**, 552–556.

41 D. H. Lim and J. Wilcox, Mechanisms of the Oxygen Reduction Reaction on Defective Graphene-Supported Pt Nanoparticles from First-Principles, *J. Phys. Chem. C*, 2012, **116**, 3653–3660.